BILINGUAL PUBLISHING CO.
Pioneer of Global Academics Since 1984

Journal of Geological Research
http://ojs.bilpublishing.com/index.php/jgr-a

ARTICLE

The Horizontal Loop Electromagnetic (HLEM) Response of Ifewara Transcurrent Fault, Southwestern Nigeria: A Computational Results

A.A. Adepelumi[1*] O.B. Olayiwola[2] D.E. Falebita[1] O.Afolabi[1] B.O Soyinka[3] J. Obokoh[4]

1.Department of Geology, Obafemi Awolowo University, Ile-Ife, Nigeria
2.Nigerian Defence Academy, Kaduna, Nigeria
3.Terracon, Seattle, Washington DC, USA
4.Sam Houston State University, Spring, Texas, USA

ARTICLE INFO

Article history
Received: 25 April 2021
Accepted: 25 May 2021
Published Online: 4 June 2021

Keywords:
Mineralized
Conductor
Overburden
HLEM
Modeling
Basement complex

ABSTRACT

The need to accurately interpret geological models that approximate mineralized zones in a Basement Complex terrain necessitate the development of horizon loop electromagnetic method (HLEM) forward modeling solutions for such scenarios. The focus of the present work is on finding rapid forward modeling solutions for synthetic HLEM data as an aid in exploration for moderate to deep conductive mineral exploration targets. The main thrust is obtaining idealized HLEM models that are required for geological interpretation of the subsurface in such environment. The original HLEM equations developed by Wesley were extended to represent a horizontally stratified earth with a conductive approximated by shear zone. From these equations a computer program was written to calculate the HLEM responses for optimal conductor model with known values of coil separations (L), depth of burial (z) and angle of dip of the target. The thin conductive model was used because it is simple and suitable for different geological scenarios. The accuracy of the approximate forward solution has been confirmed for HLEM systems with various geometric ranges, frequencies and conductivities. Three models having varying overburden thickness, dip angle of target and source-receiver separation were used in the forward modeling. The effect of varying the dip angle, overburden thickness and coil separation was studied in all the three models used. The result obtained from the forward modeling showed that variation of the dip angle gave rise to changes in the amplitudes of the anomalies generated, while that of overburden and coil separation gave rise to changes in anomaly shape. Also, the geometry and position of the causative body were precisely delineated.

1. Introduction

The main thrust of this works is the application of numeral electromagnetic forward modeling [1-16] in the mapping of geologic structure called the Ifewara transcurrent fault system (ITFS) in a study area located between 7^0 25' N - 7^0 27' N and 4^0 41' E - $4^0$42' E (Figure 1). The ITFS is situated in Ilesha area of Osun State in the southwestern

**Corresponding Author:*
A.A. Adepelumi,
Department of Geology, Obafemi Awolowo University, Ile-Ife, Nigeria;
Email: aadepelu@oauife.edu.ng

Distributed under creative commons license 4.0 DOI: https://doi.org/10.30564/jgr.v3i3.3146

part of Nigeria. It extends from Iwara through Aiyetoro to Ifewara. Three different geologic models with varying properties were used to determine the effects of conductive overburden, conductive host rock, coil separations and angle of dip on the pre-supposed fault and/or shear zone. The forward modeling code developed for this purpose is the localized, non-linear Born approximations of the 2.5D integrals of EM scattering problems [16]. Its application is based on the assumption of a wholly conductive thin conductor, whereby the HLEM anomalies are considered to be completely in-phase without a quadrature component [17].

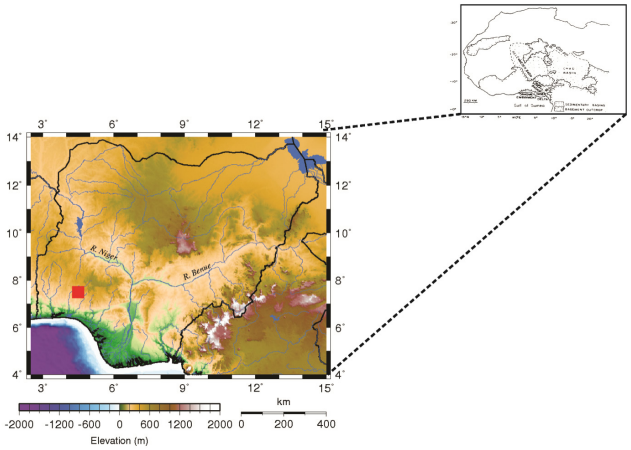

Figure 1. The location of Ifewara southwestern Nigeria inserted in the digital elevation map

The forward modelling of a thin bedrock conductor gives a trough-like HLEM anomaly whose width at the zero level equals the coil separation and the thickness of the conductor [18]. This is because there is a relationship between the geometry, depth of the conductor and the source-receiver distance of the measurement system [18]. For example, [19] has shown that clay-filled shear zones can produce spiky trough-like HLEM anomalies. However, regarding the ITFS, [20] successfully mapped the imprint of the Ifewara transcurrent fault system (ITFS), using integrated geophysical mapping methods that involved the magnetic and dipole-dipole resistivity. While [21] found extensive mylonite associated with the location of the (ITFS). They adduced the presence of this rock type is indicative of a possible fault or shear zone presence. They reported that the anomalies observed in the generated magnetic profiles correlated with the shear zones. The anomalous zone is structurally low that is gently dipping. Also, the resistivity responses obtained by [21] showed that the ITFS or shear zone is covered by thin overburden thickness, producing distinct anomaly responses. They noted that there is an inverse relationship between overburden thickness and the resolution of the resistivity images. The results of [20,21] corroborated the earlier work of [22] that employed the electrical resistivity and electromagnetic method for the detection of the ITFS and its associated possible sulphide mineralization that were earlier reported by [23].

2. Regional Geology and Tectonic Settings

The survey area falls within a region underlain by crystalline rocks that belong to the basement complex of Nigeria which forms part of the Pan-African mobile belt, east of the West African craton [20]. The common features of the Nigerian Basement Complex are polycyclicity in evolution and structural complexity due to multiple metamorphism and igneous intrusions. The earliest geologic cycle through which the rocks in this area evolved began with sedimentation [23]. This was followed by several periods of deformation that produced the gneisses and schists. The basic intrusive cycle preceded the granitic gneisses. During this cycle, a period of granitisation and deformation imparted secondary schistocity on the earlier rocks and the basic intrusives were amphibolites.

The survey area belongs to the Ife-Ilesha schist belt of southwestern Nigeria which has abundant mafic and ultramafic rocks and constitutes the upper Proterozoic schist belt of the basement complex [24,25]. Work by [26] shows that this area consists of two contrasting lithological rock association separated by a major fault called the "Ifewara fault". Detailed characteristics of the two major deformations (D1 and D2) associated with the Ifewara Shear Zone are described by [27].

3. Electromagnetic Method Overview

There are several electromagnetic techniques commonly used to delineate variations in conductivity of the earth. The conductivity is monitored on the basis of time-varying electric and magnetic fields. Maxwell's equations relate the distribution of physical property to the electromagnetic field which is a manifestation of the distribution of electric charge [16,28]. The Maxwell's equations are expressed in differential forms as equations 1 - 4.

The differential forms of the Maxwell's equations are

$$\text{rot}\,\mathrm{E} = \nabla \times \mathrm{E} = -\frac{\partial \mathrm{B}}{\partial \mathrm{t}} \quad (1)$$

$$\text{rot}\,\mathrm{H} = \nabla \times \mathrm{H} = \frac{\partial \mathrm{D}}{\partial \mathrm{t}} + \mathrm{J} \quad (2)$$

$$\text{div}\,\mathrm{B} = \nabla \cdot \mathrm{B} = 0 \quad (3)$$

$$\text{div}\,\mathrm{D} = \nabla \cdot \mathrm{D} = \mathrm{q} \quad (4)$$

Where E (V/m) is the electric field intensity vector, H (A/m) is the magnetic field intensity vector, D (C/m^2) is the electric flux density vector, B (Wb/m^2 or tesla) is the mag-

Distributed under creative commons license 4.0
DOI: https://doi.org/10.30564/jgr.v3i3.3146

netic flux density vector, J (A/m²) is the electrical current density and q = C/m^3 is the electric charge. These fields are usually functions of space (x, y, z), time t (seconds), frequency f (hertz) and angular frequency ($\omega = 2\pi f$).

Equation (1) is the Faraday's law that relates time varying magnetic field to generation of electrical voltage; Equation (2) is the Ampere's law that relates how the passage of time varying electric field leads to generation of magnetic field; Equation (3) indicates that there are no single magnetic and that the lines of magnetic induction are continuous and Equation (4) shows that electrical fields can begin and end on electrical charges which are directly related to equations 5 - 7.

$$D = \varepsilon E \quad (5)$$

$$B = \mu H \quad (6)$$

$$J = \sigma E \quad (7)$$

Where ε = electrical permittivity; μ = magnetic permeability and σ = electrical conductivity.

The commonly used small-loop EM profiling technique is the Horizontal loop electromagnetic method (HLEM). It is also known as Ronka, or MaxMin. The horizontal loop, moving transmitter and receiver, system is very flexible and used in both classic mineral exploration geophysics and in environmental and engineering applications, although different approaches to measurement are taken. The system consists of two horizontal loops, in the exploration system the loops are about a meter in diameter. For small coil separations, the loops are very small and often iron cored to achieve a high magnetic moment. In the classic systems, the coil separation is typically variable at 25, 50 or 100 m. One loop is wired to a signal generator powered by a portable battery pack. In the mineral exploration mode the generator produces currents at several frequencies in the 300 Hz - 7000 Hz range. These currents flow through the horizontal transmitter coil, giving rise to time varying magnetic fields of the same frequency. A small coil is wound around the transmitter and connected to a wire which runs to the receiver. This wire enables the phase of the signal at the receiver to be determined and ensures the transmitters and receivers are kept a fixed distance apart. The same time varying magnetic field from the transmitter intersects any conductors in the subsurface and induces an emf which in turn causes a current in the conductor as we have noted earlier. This current then causes a secondary magnetic field which intersects the receiver and induces a secondary emf [28].

4. Numerical Forward Modeling of HLEM Data

The least square algorithm developed for this study was based on the numerical forward modelling theory [16]. It was applied based on the assumption of a wholly conductive thin conductor, whereby the HLEM anomalies are considered to be completely in-phase without a quadrature component [17]. Several researchers [29,30,31,32] have used the theory which suggested the expression of normalized secondary field at the receiver coil as a percentage of the secondary field [16] as:

$$H(x) = 100\left\{\frac{L^3}{\pi}\left[\frac{tan^{-1}\left(\frac{a}{L}\right)}{L^3} - \frac{\pi}{L^3} + \frac{a}{p^2L^2}\right] + \frac{L^3}{\pi}\left[\frac{\pi}{2q^3} + \frac{tan^{-1}\left(\frac{b}{q}\right)}{q^3} + \frac{b}{q^2p^2}\right]\right.$$

$$+ \frac{L^3(q^2-3L^2)sin^2\propto}{\pi}\left[\frac{\pi}{2q^5} + \frac{tan^{-1}\left(\frac{b}{q}\right)}{q^5} + \frac{b}{q^4p^2}\right] + \frac{2L^3bsin^2\propto}{\pi q^2p^4}$$

$$[(x_t + x_r)^2 - L^2cos^2\propto] + \frac{L^3}{4\pi r_r r_t p^2}[a + bcos\,2\propto - c\,sin2\propto] +$$

$$\frac{L^3sin\propto}{\pi p^4 r_r}\left[\left((x_t + x_r) + L\cos\propto\right) \times (d\sin\propto + a\cos\propto)\right]$$

$$-\frac{L^3sin\propto}{\pi p^4 r_t}\left[\left((x_t + x_r) - L\cos\propto\right) \times (d\sin\propto - a\cos\propto)\right]$$

$$\left. + \frac{L^3}{2\pi r_r r_t p^4}[(bd^2 - ac^2)\,sin^2\propto + abc\sin 2\propto - ab(a+b)\,cos^2\propto]\right\} \quad (8)$$

Where L is the coil separation and α is the dip angle of the conductor as shown in Figure 2. Other notations used for simplifying equation (8) are as follows:

$x_r = (x - x_o)\,cos\propto + z\,sin\propto + \frac{L}{2}\cos\propto$; $x_t = (x - x_o)\,cos\propto + z\,sin\propto - \frac{L}{2}\cos\propto$; $z_r = z\,cos\propto - (x - x_o)\,sin\propto - \frac{L}{2}sin\propto$; $z_t = z\,cos\propto - (x - x_o)\,sin\propto + \frac{L}{2}sin\propto$; $r_r = \sqrt{x_r^2 + z_r^2}$; $r_t = \sqrt{x_t^2 + z_t^2}$; $a = 2\sqrt{r_r r_t}\,cos\left(\frac{\emptyset_r - \emptyset_t}{2}\right)$; $b = 2\sqrt{r_r r_t}\,cos\left(\frac{\emptyset_r + \emptyset_t - 3\pi}{2}\right)$; $c = 2\sqrt{r_r r_t}\,cos\left(\frac{\emptyset_r + \emptyset_t}{2}\right)$; $d = 2\sqrt{r_r r_t}\,cos\left(\frac{\emptyset_r - \emptyset_t - 3\pi}{2}\right)$; $p = \sqrt{L^2 + a^2}$; $q = \sqrt{(x_t + x_r)^2 + (L\,sin\propto)^2}$; $z_r < 0 \Rightarrow \emptyset_r = -\frac{\pi}{2} - tan^{-1}\frac{x_r}{z_r}$; $z_r > 0 \Rightarrow \emptyset_r = \frac{\pi}{2} - tan^{-1}\frac{x_r}{z_r}$; $z_t < 0 \Rightarrow \emptyset_t = -\frac{\pi}{2} - tan^{-1}\frac{x_t}{z_t}$; $z_t > 0 \Rightarrow \emptyset_t = \frac{\pi}{2} - tan^{-1}\frac{x_t}{z_t}$;

where the dip angle of the conductor α should be in the range of 0^0 - 90^0 [16] and x is midpoint between transmitter and receiver coils.

Distributed under creative commons license 4.0 DOI: https://doi.org/10.30564/jgr.v3i3.3146

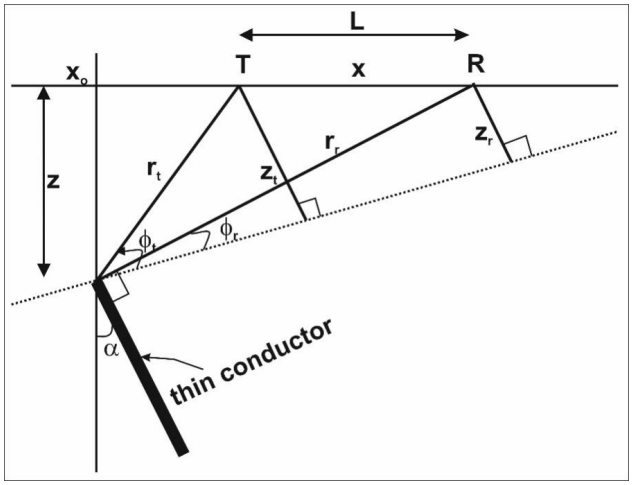

Figure 2. Geometrical relationship between transmitter T, receiver R and the thin conductor with infinite extent (modified after [29] and [30]). Optimized parameters are the burial depth (z), dip angle (α) and surface projection point (x_0)

4.1 The Models

In order to predict the characteristic response of the conductive target (Ifewara fault), theoretical anomalies were produced using equation 8 for coil separations of L = 50 m, 100 m, and 150 m (Table 1). The angle of dip of the target was varied from 0^0 to 90^0 with 5^0 increments. Forward modeling was carried out using five different overburden depth which are z = 10 m, 20 m, 30 m, 40 m and 50 m, while the projection point to the surface (x_o) was 225 m. The characteristics of the slingram (HLEM) profiles are determined by the geometry of the receiver and transmitter coils as well as geometry and attitude of the conductive source. It is expected that the response of a vertically oriented plate-like conductive body would appear as a negative peak, approximately 1.3 times the coil separation distance with two lower amplitude positive shoulders on either side [28].

Table 1. Model parameters

Parameters	Model	1	2	3
T - R coil separation (L)	A	50 m	100 m	150 m
Surface projection (x_o)	B	225 m	225 m	225 m
Profile length	C	500 m	500 m	500 m
Angle of dip (α)	D	0^o - 90^o step 5^o	0^o - 90^o step 5^o	0^o - 90^o step 5^o
Depth of burial (z)	E	10 - 50 m	10 - 50 m	10 - 50 m

5. Discussion of Results

5.1 Forward Modeling

The synthetic anomaly signatures obtained for Model 1 are shown in Figures 3 (a - e). It is obvious from the figures that the amplitudes of the anomaly changes with change in the angle of dip. As the angle of dip increases from 0^0 to 90^0, amplitudes of the anomaly is observed to be rising on the down dip side of the conductive target, while the amplitudes on the up dip side becomes flattened (decreased) gradually. At dip angle of 90^0, a vertically dipping target, the amplitudes of the anomaly curve are observed wide apart. While one arm has its maximum value to be positive, the other has it to be negative. It can be observed also, that with a change in the value of the overburden thickness but with the same coil spacing, the behaviour of the arms of the anomaly was observed to change compared to that of model 1A. This change in behaviour is deduced to be solely due to the change in the overburden thickness. From the figure, it is obvious that the change in behaviour is conspicuous when the conductive target is dipping at angle of 90^0 as one of the peak amplitudes of the anomaly for Model 1A (Figure 3a) is negative while both peak amplitudes in the case of Model 1B are positive. Furthermore, it is observed that the increase in overburden thickness from 10 m to 20 m significantly affected the anomaly response obtained. This shows that overburden thickness affects the amplitude of slingram responses. The interpretation of these anomalies are similar to those above except that the peak positive and negative amplitudes of the slingram response has reduce to as low as 10 and -5 respectively unlike in Model 1A (Figure 3a) where the overburden thickness is very shallow and the transmitted wave is able to induce substantial secondary signal in the conductor.

In Figure 3d (Model 1D), the effect of the overburden is further observed on the slingram response. As the overburden increases to 40 m, the peak negative response increases to -3, while that of positive response reduces to about 10. The effect of this is that transmitted signal getting to the conductor is small hence its response is also minute. The effect of increased overburden depth led to lower slingram response to about 4 and -1.5 (See Figure 3e, Model 1E) for peak positive and negative amplitudes respectively; this indicates that the conductor has been energized by small quantity of the signal. In this case the overburden depth is 50 m.

Similar interpretation can be given to Figure 4a just like in Model 1A (Figure 3a) interpretation except that the width of the anomaly is wider compared to the former. The slingram responses are high just as in the case of Model 1A

Distributed under creative commons license 4.0
DOI: https://doi.org/10.30564/jgr.v3i3.3146

which shows that large quantity of the signal energized the conductor due to small overburden effect but larger width is attributed to increase in Transmitter - Receiver coil separation which is 100 m while that of Model 1A is 50 m both with overburden of 10 m. In Figure 4b, the effect of increased overburden depth and increased T - R coil separation is observed further and the width of the anomaly has reduced due to the increment in the overburden depth. The values of the response have also decreased implying that the conductor is being energized by lesser signal compared to that of Model 2A (Figure 4a). In Figure 4c, the width of the anomaly is further reduced as the overburden depth is increased. Just as in others, the amplitudes of the anomaly is symmetrical for a vertical conductor, while the amplitude increases on the down dip side and decreases on the up dip side showing an asymmetric shape. At 90^0, one of the amplitudes is negative while the other is positive. In Figure 4d, it is evident that the width of the anomaly is further reduced while other interpretations are similar to the above except that at 90^0, both amplitudes are positive. Similarly, the anomalies shown in Figure 4e shows a different signature compared to that of Model 1E above. The slingram responses are relatively higher. They range from -7 to - 10 for the peak negative, while those of peak positive ranges from 5 to 20; compared to that of Model 1E (Figure 3e) where we have peak negative to range from -0.5 to -1.5 and peak positive to range from 1 to 3. This shows that the coil separation influences the depth of penetration of the signal with the same frequency.

With increase in the Transmitter - Receiver coil separation to 150 m, and varying the overburden depth from 10 m to 50 m, EM response that is different from other models was observed (Figure 5a). The widths of the anomalies are observed to be wider compared to those of other two models connoting that the coil separation affect the shape of the anomaly and the longer the coil separation the wider the width of the anomaly for the same overburden depth. In Figure 5b, it is observed that increase in the overburden depth from 10 m to 20 m for the same coil separation led to decrease in the width of the anomaly. Also, the slingram (HLEM) responses are much higher than the previous models for the same overburden depth; the significant of this is that the increased coil separation enhanced energization of the conductor. This modeling result shown in Figure 5c is similar to those of Figure 5b except that the width of the anomaly is further reduced due to increase in the overburden depth and reduction in the slingram responses showing that, lesser signal energizes the conductor. The effect of varying the dip angle is observed as the symmetry of the anomaly changes from symmetrical for vertical conductor with dip angle of zero degree to asymmetrical as the angle increases from 0 to 90 degrees. The effect of increased coil separation on the slingram responses is worthy of note here (Figure 5d). The slingram responses obtained in Figure 5d compared moderately well to the previous models (Figure 5c) for the same overburden depth is observed to be increasing with increasing coil separation. This implies that the higher the coil separation, the higher the energization of conductors for the same value of frequency. Also the width of the anomaly is further increased. Reduction in the width of the anomaly as a result of increase in the coil separation observed in Figure 5e possibly lead to the deduction that the width of the anomaly is dependent on the energization of the conductor. With high energization of the conductor, the peak negative width of the anomaly is high, while it is low for low energization. Effect of coil separation is mainly in enhancement of depth of investigation while that of dip is observed in the symmetry of the anomaly.

5.2 Effect of Conductive Overburden

In our study, the effects of overburden on the buried conductors(s) are explained using the forward modeling results shown in Figure 6 (a - d) respectively. Overburden layer is that layer enclosing the conductor from the top whose thickness can either or not be in contact with the conductor. Conductively coupling occurs when an overburden is in galvanic contact with the conductor. While inductively coupling occurs when an overburden does not have any contact with the conductor [28,33].

Figure 6 (a - d) shows slingram (HLEM) curves for 0^o, 30^o, 60^o, and 90^o dips and the effect of overburden depths of 10, 20, 30, 40, and 50 m plotted for each dip angle. In all cases, the conductor is located directly below the peak negative of the anomaly. Also, it is apparent from the figures that the smaller the overburden thickness to the conductor, the higher the anomaly response and vice-versa. In contrast, the higher the dip angle, the greater the amplitude and the asymmetry of the anomaly curves are much more pronounced at shallower depths. For example, the updip peak and downdip trough are sharper and broader respectively at 10 m than at 50 m. According to [34], if an overburden of appreciable response parameter is present (although neglected) as one makes an interpretation for the depth of a conductor, it appears as if the target is deeply buried and a better conductor than it actually is. The results obtained in this research confirm the observations of [35] that an increase in the conductance of an inductively coupled overburden layer will lead to a decrease in the horizontal loop EM anomaly.

5.3 Effect of Conductive Host Rock

The typical model [36] of an EM response of a conductor

Distributed under creative commons license 4.0 DOI: https://doi.org/10.30564/jgr.v3i3.3146

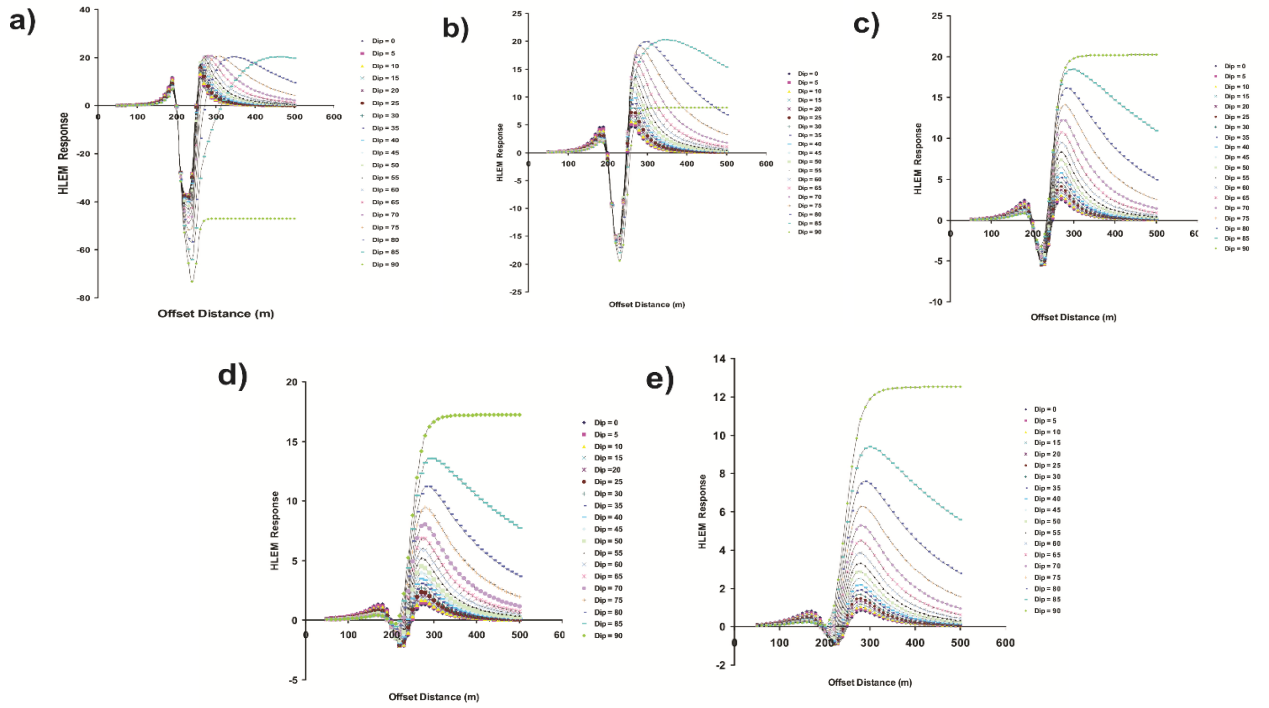

Figure 3. Superposition of HLEM anomaly responses for Model 1A (upper left panel), Model 1B (middle left panel), Model 1C (lower left panel), Model 1D (upper right panel) and Model 1E (middle right panel) with target dipping between 0 and 90 degrees, and depth of burial of 10 m, 20 m, 30 m, 40 m and 50 m, and T - R separation of 50 m. The plot shows the effect of varying dip angle of conductor on slingram response.

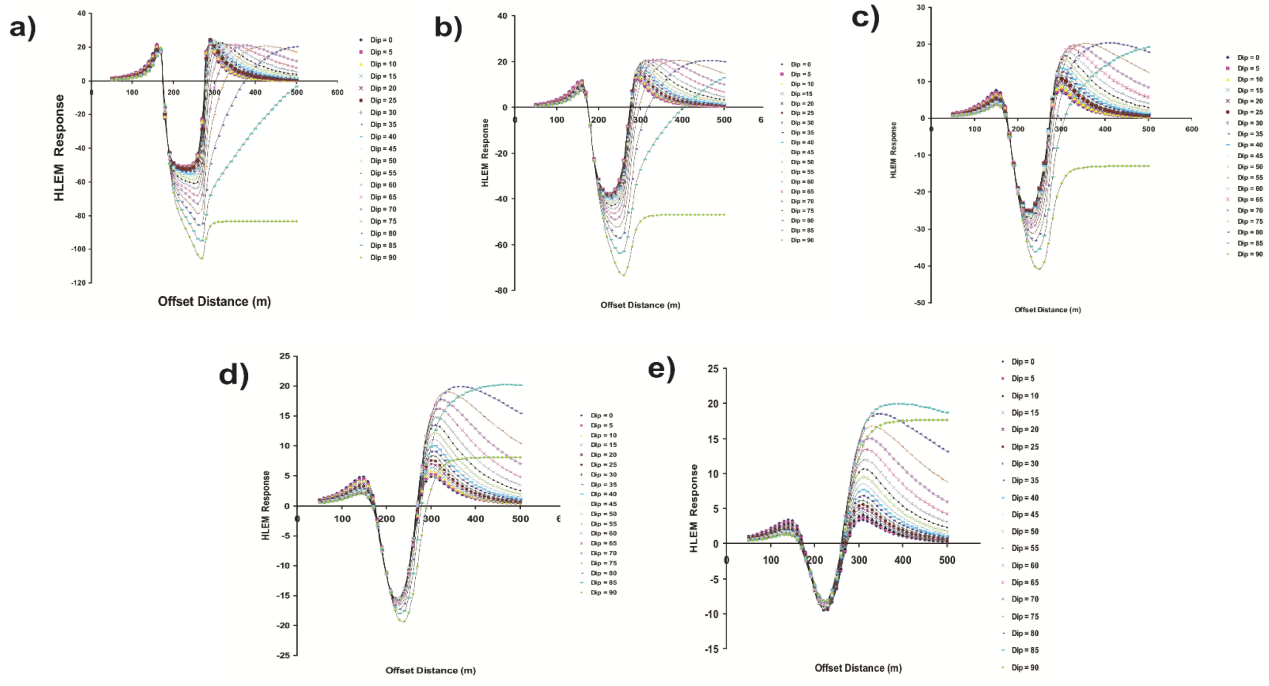

Figure 4. Superposition of HLEM anomaly responses for Model 2A (upper left panel), Model 2B (middle left panel), Model 2C (lower left panel), Model 2D (upper right panel) and Model 2E (middle right panel) with target dipping between 0 and 90 degrees, and depth of burial of 10 m, 20 m, 30 m, 40 m and 50 m, and T - R separatioon of 50 m. The plot shows the effect of varying dip angle of conductor on slingram response.

Distributed under creative commons license 4.0
DOI: https://doi.org/10.30564/jgr.v3i3.3146

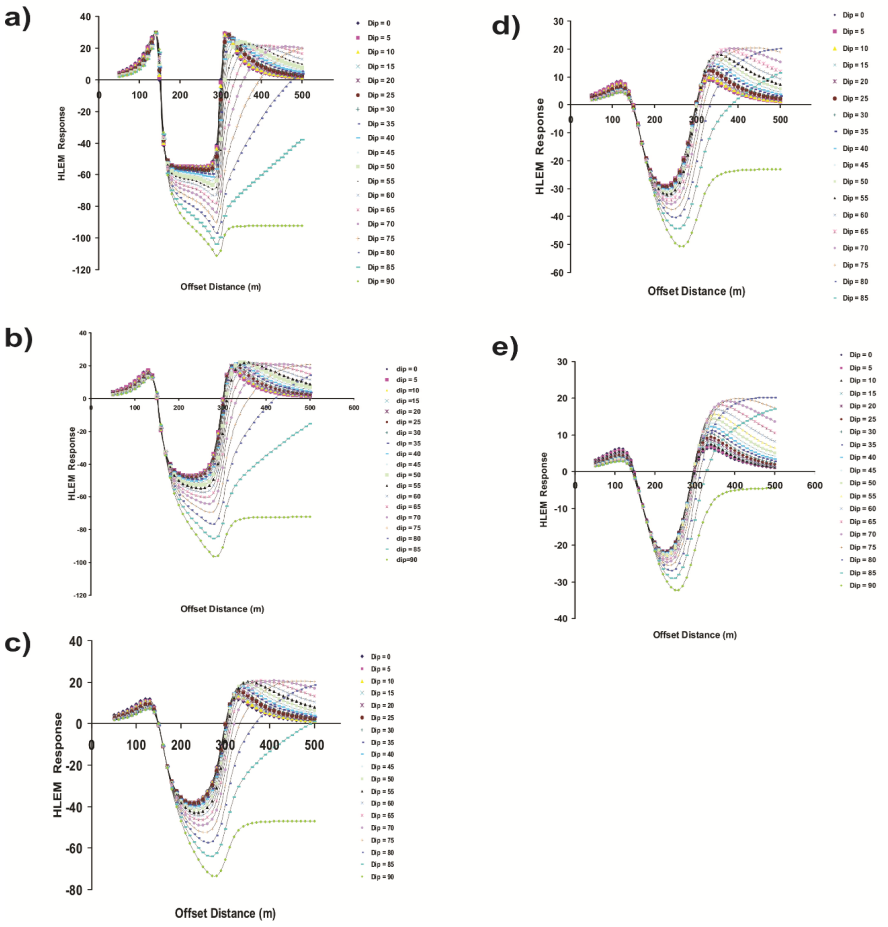

Figure 5. Superposition of HLEM anomaly responses for Model 3A (upper left panel), Model 3B (middle left panel), Model 3C (lower left panel), Model 3D (upper right panel) and Model 3E (middle right panel) with target dipping between 0 and 90 degrees, and depth of burial of 10 m, 20 m, 30 m, 40 m and 50 m, and T - R separation of 50 m. The plot shows the effect of varying dip angle of conductor on slingram response.

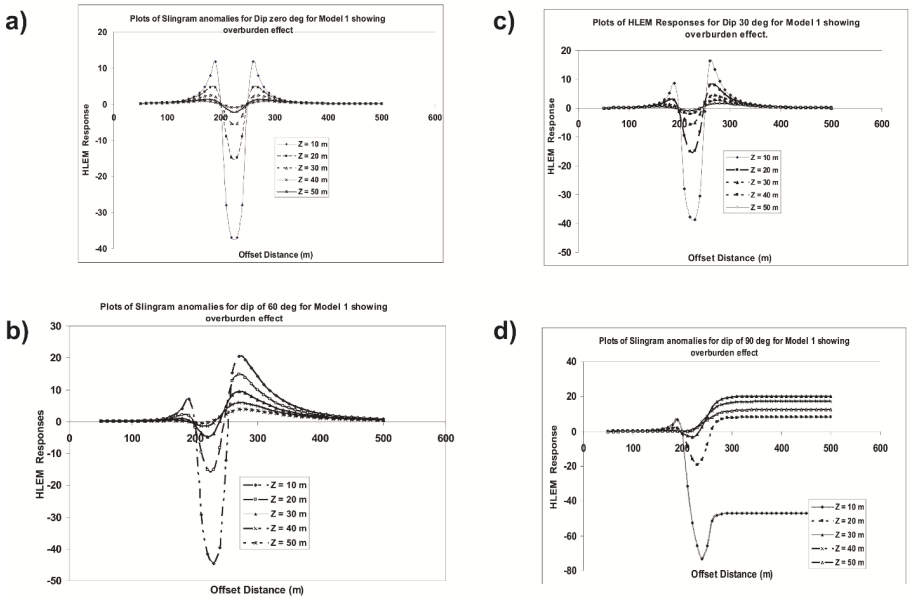

Figure 6. Slingram (HLEM) anomalies showing the overburden effect on the conductor. (0° dip in upper left panel), (30° dip in lower left panel), (60° dip in upper right panel) and (90° dip in lower left panel).

enclosed by a conductive host rock is described by the dual of 'vortex' and 'galvanic' currents. The galvanic current dominates when the host rock is conductive while the vortex current dominates when the host rock is resistive. If the galvanic current dominates, only the location and depth of the buried conductor are determined. This is probably because buried conductor can generate natural telluric currents in the host and thus result in upsurge of ambient noise [37,38]. The conductor would then appear to be shallower and more resistive than it is actually. Comparing the responses of the broadside and in-line horizontal loop EM (slingram) configurations may help to resolve the ambiguities [39]. According to [40] the effects of the conductivity of a host rock on the horizontal loop response of a conductor with known conductivity for a homogenous half-space are in four parts. The first part describes an initial effect when the conductivity of the host increases from zero. There is a slight anticlockwise phase rotation of the anomaly as a result of the passage of quadrature currents from the host to the conductor. This means there is an enhancement of anomaly due to upsurge in scatter current density. The second part indicates that as the conductivity of the host continues to increase, there is a higher enhancement of the anomaly till it is about twice the response in free space. This is because there will be a clockwise phase rotation as a result of the phase shifts in the primary field. Further increase in the host conductivity leads to extra clockwise phase rotations and anomaly attenuation. These effects are as a result of losses experienced as the primary field travels to the conductor and as the secondary field travels from the conductor to the receiver. It should be noted that high frequency may not be enough to resolve significant target when using horizontal loop. This is because small lateral inhomogeneities in the conductivity of the host may create very profound effects. For this present study, the effect of the conductive host rock was not computed by us because that has been done by [30].

5.4 Effects of Coil Separation on the Buried Conductor

In other to examine the effects of coil separation (L) on the horizontal loop EM signature, for a vertical conductor buried at depth of 10 and 50 m, anomalies for coil separations (L) of 50, 100 and 150 m were computed and plotted together at dip angles of 0^o, 45^o and 90^o. The results obtained showed that the width of the main negative slingram anomaly clearly varies with the coil separation Figure 7 (a - f). The major effect of coil separation on slingram signature is the broadening of the anomaly and deeper penetration of depth of investigation. The implication of this is proper energization of the conductor in the subsurface as the coil separation is increased.

5.5 Effects of Dip on the Buried Conductor

Figure 8 (a - d) show the computed anomalies for a coil separation of L = 50 m with the target conductor at depths of z = 10, 20, 30, 40 and 50 m, dipping at d = 0^o, 30^o, 60^o and 90^o.

It can be observed that the anomalies are more symmetrical at lower angles and become increasingly asymmetrical as the angle increases (Figure 8a - d). Also, at smaller depth, the amplitude of the anomalies at the updip side is higher than that at the downdip side. However, as the depth increases (e.g. z = 30, 40, and 50, Figure 8d) the reverse is the case with respect to the amplitude. This confirms that horizontal loop EM anomalies lose their asymmetry and position of their peak amplitude at increasing depth for dipping conductor [41].

6. Conclusions

This study has attempted to characterize different geologic scenarios through model simulation of overburden occurrence, coil separation and dip in identifying mineralized zones using HLEM methods. The overburden thickness (z) of 10 m, 20 m, 30 m, 40 m, 50 m; having coil separation (L) of 50 m, 100 m, 150 m, and dip angle (α) that varies from 0^o to 90^o were used to constrain the models employed. This was done to investigate the effectiveness of horizontal loop electromagnetic method (HLEM) in mapping the mineralized Ifewara transcurrent fault/shear zone within the typical basement complex terrain of southwestern Nigeria.

We observed that the overburden layer is a major attenuator of the amplitude of HLEM anomalies. This result implies that in a typical HLEM survey, consideration must be given to the possibility of both conductive and inductive effect of the overburden on the conductor. Generally, different coil separations control the observed width of the anomalies and the depth of investigation; therefore, choosing appropriate coil separation is expedient when HLEM is used for mineral exploration. Doing this would assist in overcoming the high absorption of HLEM signals posed by the thick overburden overlying the conductor being investigated. On the other hand, as the dip angle increases, the HLEM responses become more asymmetrical as it deviates from vertical. High amplitude ratios of the HLEM anomaly indicate good conductivities. The relative amplitude of the responses is related to the depth of the conductor. Depth to the conductive source can be estimated from the amplitude of the responses obtained from the forward modeling. The depth of investigation is observed to be mainly dependent upon the frequency, coil separation, overburden thickness, and host conductivity. It is concluded that the methodology presented may provide a useful basis for the quantitative interpretation of HLEM data in similar terrain as considered in this study.

Distributed under creative commons license 4.0
DOI: https://doi.org/10.30564/jgr.v3i3.3146

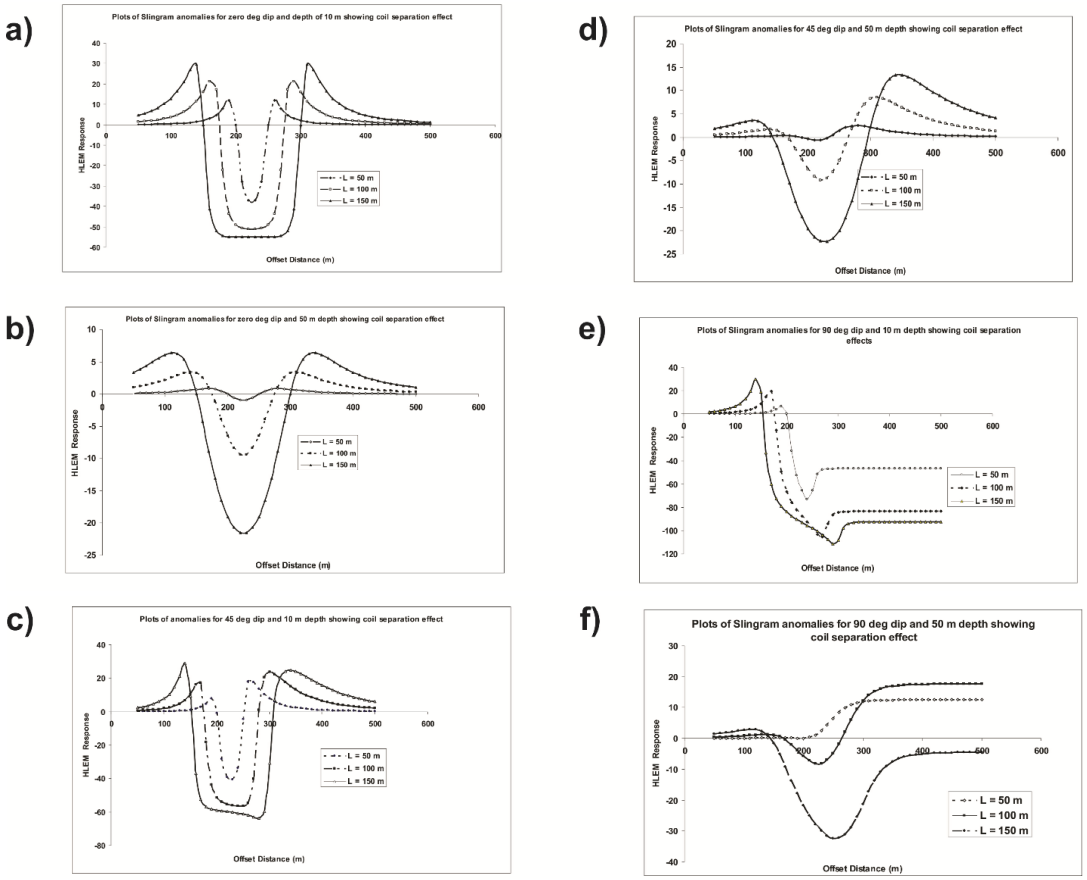

Figure 7. Slingram (HLEM) anomalies for vertically dipping conductor with varying coil separation L = 50, 100 and 150 m and conductor depth of 10 m depth (upper left panel); at 50 m depth (middle left panel). With the same coil separation, conductor dipping at 45^0 and overburden thickness of 10 m (lower left panel); at 50 m (upper right panel). Also with the same coil separation, horizontal conductor and overburden thickness of 10 m (middle right panel); and at 50 m (lower right panel).

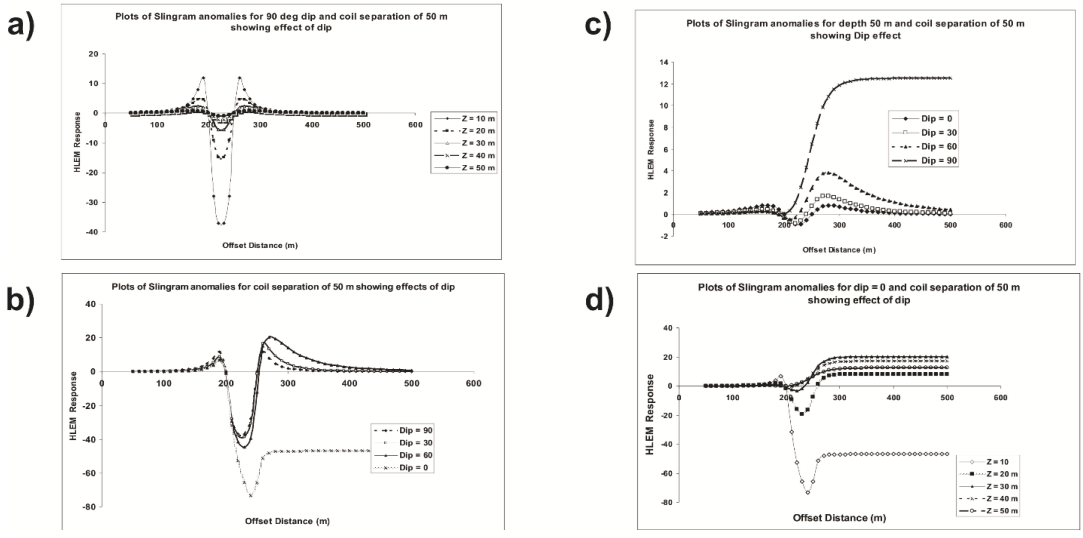

Figure 8. Slingram (HLEM) anomalies for vertically dipping conductor buried at 10, 20, 30, 40 and 50 m with coil separation of 50 m (upper left panel); vertical conductor buried at 10m depth with varying dip angle of 0^o, 30^o, 60^o and 90^o and coil separation of 50 m (lower left panel); vertical conductor buried at 50 m depth with coil separation of 50 m and varying dip angle of 0^o, 30^o, 60^o and 90^o (upper right panel); and horizontal conductor buried at 10, 20, 30, 40 and 50 m with coil separation of 50 m (lower right panel).

Distributed under creative commons license 4.0 DOI: https://doi.org/10.30564/jgr.v3i3.3146

References

[1] Ward, S. H., and Gledhill, T., (1957), Electromagnetic Surveying-ground methods, in Methods and case histories in mining geophysics: Bull. Can. Inst. Min. Metallurg., 63-70.

[2] Ward., S. H. and Hohmann., G. W. 1988. Electromagnetic Theory for Geophysical Applications, in Electromagnetic Methods in Applied Geophysics—Theory," Society of Exploration Geophysicists, Tulsa, Vol. 1, 1988, pp. 131- 311.

[3] Spies, B. R., and Frischknecht, F. C., 1991. Electromagnetic sounding. In: Nabighian MN (ed) Electromagnetic methods in applied geophysics, Volume 2, Applications. Society of Exploration Geophysics., Tulsa, 285-425.

[4] Wannamaker, P. E., Hohmann, G. W., and San-Filipo, W. A., 1984. Electromagnetic modeling of three-dimensional bodies in layered earths using integral equations. Geophysics, 49, 60-74.

[5] Newman, G. A., and Hohmann, G. W., 1988. Transient electromagnetic responses of high-contrast prisms in a layered earth. Geophysics, 53, 691-706.

[6] Lee, K. H., Liu, G., and Morrison, H. F., 1989. A new approach to modeling the electromagnetic response of conductive media. Geophysics, 54, 1180-1192.

[7] Xiong, Z., 1992. Electromagnetic modeling of three-dimensional structures by the method of system iteration using integral equations. Geophysics, 57, 1556-1561.

[8] Wang, T. and Hohmann, G. W., 1988. 'A finite-difference time-domain solution for three-dimensional electromagnetic modeling', Geophysics, 58, 797-809.

[9] Mackie, R. L., Madden, T. R., and Wannamaker, P. E., 1993. Three-dimensional magneto-telluric modeling using difference equations. Geophysics, 58, 215-226.

[10] Torres-Verdín, C., and Habashy, T. M., 1994. Rapid 2.5-dimensional forward modeling and inversion via a new nonlinear scattering approximation. Radio Science, 29, 1051-1079.

[11] Zhdanov, M. S., and Fang, S., 1996. 'Quasi-linear approximation in 3-D electromagnetic modeling', Geophysics, 61, 646-665.

[12] Liu, E. H., and Lamontage, Y., 1998. Geophysical application of a new surface integral equation method for EM modeling. Geophysics, 63, 411-423.

[13] Mitsuhata, Y., 2000. 2-D electromagnetic modeling by finite-element method with a dipole source and topography. Geophysics, 65, 465-475.

[14] Sasaki, K., 2001. Full 3-D inversion of electromagnetic data on PC. Journal of Applied Geophysics, 46:, 45-54.

[15] Hohmann, G. W., 1988. Numerical Modelling for Electromagnetic methods in geophysics in Nabighian, M. N., Ed., Electromagnetic methods in geophysics, Vol. 1, Soc. Explorations Geophysics. 313-363.

[16] Wesley, J. P., 1958. Response of a dike to an oscillating dipole. Geophysics, 23 (1), 128-133.

[17] Parasnis, D. S., (1971), Analysis of some multi-frequency, multiseparation electromagnetic surveys: Geophysical Prospecting, 19, 163-179.

[18] Telford, W. M., Geldart,L.P., Sheriff, R.E and Keys, D. A., 1976. Applied Geophysics, Cambridge University Press, 250 - 270.

[19] Palacky, G. J., Ritsema, I. L., and De Jong, S. J., 1981. Electromagnetic prospecting for groundwater in Precambrian terrains in the Republic of Upper Volta: Geophysical Prospecting, 29, p. 932-955.

[20] Adepelumi, A. A., Ako, B. D., Ajayi, T. R., Olorunfemi, A. O., Awoyemi, M. O and Falebita. D. E., 2008. Integrated geophysical mapping of the Ifewara transcurrent fault system, Nigeria. Journal of African Earth Sciences, 52 (4-5), 161-166.

[21] Akinde., A. S., Adepelumi, A .A and Dikedi., P. N., 2019. IFEWARA MYLONITE: Identifying the Neo-Tectonic Overprint Using Integrated Geophysical. Journal of Geology and Geophysics, 8 (2) 458, 1 -12.

[22] A Ako, B.D., Ajayi, T.R. and Alabi, A.O. (1978): A geochemical study of Ifewara area. Journal of Mining and Geology, Vol. 15(2), pp. 85 - 90.

[23] De Swardt, A.M.J. (1953): The geology of the country around Ilesha.Geological Survey of Nigeria, Bulletin. No. 23, pp 1-54.

[24] Elueze, A. A. (1982). Metallographic studies of ore minerals in the amphibolites of llesha Schist belts, southwestern Nigeria. Nigerian Journal Mining Geology, 19, 53-58.

[25] Turner, D.C. 1983. Recent advances in the study of the basement Complex of Nigeria. In: Oluyide P.O., et. al. (Eds). Precambrian Geology of Nigeria. Geology survey of Nigeria, 11 - 43.

[26] Rahaman, M.A. (1988): Recent Advances in the Study of the Basement Complex of Nigeria. In Precambrian Geology of Nigeria. Geological Survey of Nigeria, 11 - 41.

[27] Caby R., and Boesse J.M., (2001), Pan-African nappe system in southwest Nigeria: the Ife-llesha schist belt. Journal of African Earth Sciences, Vol 33, 2, 21 l-225.

[28] Frischknetch, F. C., Labson, V. F., Spies, B. R., and Anderson, W. L., 1991. Profiling Methods Using

Distributed under creative commons license 4.0
DOI: https://doi.org/10.30564/jgr.v3i3.3146

Small Sources: Electromagnetic Methods in Applied Geophysics, Vol. 2, Application, Parts A and B, 105-270.

[29] Dondurur, D., and Sari, C., 2004. A Fortran 77 Computer Code for Damped Least-squares Inversion of Slingram Electromagnetic Anomalies over Thin Tabular Conductors: Computers and Geosciences, 30, 591-599.

[30] Duckworth, K., Krebes, E.S., 1995. A Quickbasic program for the computation of the response of a thin tabular perfect conductor to a two coil horizontal coplanar electromagnetic prospecting system. Computers & Geosciences 21 (2), 333-343.

[31] Duckworth, K., and O'Neil, D. A., 1989. Turam responses in a scale model conductive environment for single and paired conductors. Canada Journal of Exploration Geophysicists, 25. 115-137.

[32] Duckworth, K., Calvert, H.T., Juigalli, J., 1991. A method for obtaining depth estimates from the geometry of Slingram profiles. Geophysics, 56 (10), 1543-1552.

[33] Joshi, M. S., Gupta, O. P and Negi, J. G., 1988. On the effects of thickness of the half-plane model in HLEM induction prospecting over sulphide dykes in a highly resistive medium. Geophysical Prospecting, 36, 551-558.

[34] Lowrie, W., and West, G. F., (1965), The effect of a conductive overburden on electromagnetic prospecting measurements. Geophysics, 30 (4), 624-632.

[35] Poddar, M., 1982. Interpretation of pulse EM anomalies over Gani conductors: Geophysical Prospecting. 30, 86-100.

[36] McNeill, J. D., Edwards, R. N., and Levy, G. M., 1984. Approximate calculations of the transient electromagnetic response from buried conductors in a conductive half-space: Geophysics, 49, 918-924.

[37] Lilley, F. E. M., and Woods, D. V., 1978. The channeling of natural electrics by orebodies: Bulletin of Australian Society of Exploration Geophysics., 9, 62-63.

[38] Negi, J. G., Gupta, O. P., and Joshi, M. S., 1987. Corrections for conductivity estimates in induction prospecting of sulphide-dykes in a layered environment: Geophysical Prospecting, 35, 718-734.

[39] Gupta, 0. P., Joshi, M. S., and Negi, J. G., 1980. Scale model electromagnetic response to inline and broadside systems at skew traverses of a dipping half-plane embedded in a conductive host rock: Geophysical Prospecting, pp.119-134.

[40] Hanneson, J.E., West, G.F., 1984. The horizontal loop electromagnetic response of a thin plate in a conductive earth: Part II—computational results and examples. Geophysics 49 (4), 421-432.

[41] Dondurur., D (2005), Depth Estimates for Slingram Electromagnetic Anomalies from Dipping Sheet-like Bodies by the Normalized Full Gradient Method: Pure and applied geophysics, 162, 2179-2195.

Distributed under creative commons license 4.0 DOI: https://doi.org/10.30564/jgr.v3i3.3146